Laning and clustering transitions in driven binary active matter systems

C. Reichhardt,[1] J. Thibault,[1,2] S. Papanikolaou,[2,3] and C. J. O. Reichhardt[1]
[1]*Theoretical Division and Center for Nonlinear Studies, Los Alamos National Laboratory, Los Alamos, New Mexico 87545, USA*
[2]*Department of Mechanical and Aerospace Engineering, Western Virginia University, Morgantown, West Virginia 26506, USA*
[3]*Department of Physics, Western Virginia University, Morgantown, West Virginia 26506, USA*

(Received 17 May 2018; published 7 August 2018)

It is well known that a binary system of nonactive disks that experience driving in opposite directions exhibits jammed, phase separated, disordered, and laning states. In active matter systems, such as a crowd of pedestrians, driving in opposite directions is common and relevant, especially in conditions which are characterized by high pedestrian density and emergency. In such cases, the transition from laning to disordered states may be associated with the onset of a panic state. We simulate a laning system containing active disks that obey run-and-tumble dynamics, and we measure the drift mobility and structure as a function of run length, disk density, and drift force. The activity of each disk can be quantified based on the correlation timescale of the velocity vector. We find that in some cases, increasing the activity can increase the system mobility by breaking up jammed configurations; however, an activity level that is too high can reduce the mobility by increasing the probability of disk-disk collisions. In the laning state, the increase of activity induces a sharp transition to a disordered strongly fluctuating state with reduced mobility. We identify a novel drive-induced clustered laning state that remains stable even at densities below the activity-induced clustering transition of the undriven system. We map out the dynamic phase diagrams highlighting transitions between the different phases as a function of activity, drive, and density.

DOI: 10.1103/PhysRevE.98.022603

I. INTRODUCTION

A binary assembly of interacting particles that couple with opposite sign to an external drive such that the two particle species move in opposite directions has been shown to exhibit a rich variety of dynamical behaviors [1–3], the most striking of which is a transition to a laning state in which high mobility is achieved through organization of the particles into noncolliding chains [3–8]. Such systems have been experimentally realized using certain types of colloidal particles [9–11] or dusty plasmas [12,13] and have been used as a model for motion in social systems ranging from pedestrian flow [2,14] to insect movement [15]. A variety of nonlaning states can appear in these systems, including jammed states where the particles block each other's motion [16–19], pattern forming states [19–25], and fully phase-separated states [17–19]. The laning transition has many similarities to the phase separating patterns observed in related driven binary systems, indicating that formation of such patterns is a general phenomenon occurring in many nonequilibrium systems [26–29]. In a recent study of nonactive binary disks driven in opposite directions, a comparison of the velocity force curves with those found in systems that exhibit depinning behavior revealed four dynamic phases: a jammed state, a fully phase-separated high-mobility state, a lower mobility disordered fluctuating state, and a laning state [19]. The transitions between these phases as a function of increasing drift force appear as jumps or features in the velocity force curves coinciding with changes in the structural order of the system [19].

Active matter, consisting of particles that can propel themselves independently of externally applied forces, is an inherently nonequilibrium system commonly modeled using either driven diffusive or run-and-tumble dynamics [30,31]. For sufficiently large activity, such systems are known to undergo a transition from a uniform fluid state to a phase separated or clustered state [32–38]. The onset of clustering or swarming can strongly affect the overall mobility of the particles when obstacles or pinning are present [39–44]. In studies of active matter moving under a drift force through obstacles, the mobility is maximized at an optimal run length since small levels of activity can break apart the clogging or jamming induced by the quenched disorder, but high levels of activity generate self-induced clustering that reduces the mobility [44,45].

In this work, we examine a binary system of oppositely driven active run-and-tumble particles. In the absence of activity, such a system is known to exhibit lane formation, but we find that when activity is included, several new dynamic phases appear. Adding activity to the nonactive jammed state can break apart the jammed structures and restore the mobility to finite values, while when the nonactive phase-separated state is made active, the system becomes susceptible to jamming or clogging through a freezing-by-heating effect [2]. High levels of activity generally decrease the mobility by producing a disordered partially clustered fluctuating state. The mobility of the nonactive disordered state decreases when activity is added, while the nonactive laning states undergo a sharp transition as the activity is increased from low-collision, high-mobility lanes to a low-mobility disordered state with frequent particle collisions. At high drives and large activity, we find a new phase that we term a *laning cluster phase* in which dense clusters appear that are phase separated into the two different, oppositely driven species. The laning cluster phase is stable down to particle densities well below the onset of activity-induced clustering in an undriven system. Transitions among these different phases can be identified through changes in mobility, changes in the particle structure, or changes in the frequency of particle-particle collisions, and we use these changes to map the dynamic phases as a function of external drift force, density, and activity. We draw analogies between the sharp transition we observe from the high-mobility laning state to the low-mobility disordered fluctuating state and panic transitions in which a high-mobility state of pedestrian flow can change into a low-mobility panic state in which continuous collisions between pedestrians occur.

We note that previous work on oppositely driven active matter particles by Bain and Bartolo [46] focused on the nature of the critical behavior at the transition between a fully phase separated state and a disordered mixed phase, rather than the mobility that we consider. Reference [46] also uses a flocking or Vicsek model, which is distinct from the run-and-tumble or driven diffusive active matter systems that are the focus of our work.

II. SIMULATION AND SYSTEM

We consider a two-dimensional system of size $L \times L$ with periodic boundary conditions in the x and y directions containing N particles of radius R_d. We take $L = 36$ and $R_d = 0.5$. The interaction between particles i and j has the repulsive harmonic form $\mathbf{F}_{pp}^{ij} = k(r_{ij} - 2R_d)\Theta(r_{ij} - 2R_d)\hat{\mathbf{r}}_{ij}$, where $r_{ij} = |\mathbf{r}_i - \mathbf{r}_j|$, $\hat{\mathbf{r}}_{ij} = (\mathbf{r}_i - \mathbf{r}_j)/r_{ij}$, and Θ is the Heaviside step function. We set the spring stiffness $k = 50$, large enough that there is less than a 1% overlap between the particles, placing us in the hard disk limit as confirmed in previous works [11,12,37]. The area coverage of the particles is $\phi = N\pi R_d^2/L^2$, and a triangular solid forms for $\phi = 0.9$ [37]. The particles are initialized in nonoverlapping randomly chosen locations and are coupled to an external dc drift force $\mathbf{F}_d = \sigma_i F_d \hat{\mathbf{x}}$, where $\sigma_i = +1$ for half of the particles, chosen at random, and $\sigma_i = -1$ for the remaining half of the particles. The dynamics of particle i are determined by the following overdamped equation of motion:

$$\eta \frac{d\mathbf{r}_i}{dt} = \sum_{j\neq i}^{N} \mathbf{F}_{pp}^{ij} + \mathbf{F}_d + \mathbf{F}_m^i. \tag{1}$$

Each particle experiences a motor force $\mathbf{F}_m^i = F_m\hat{\xi}$ which propels the particle in a randomly chosen direction $\hat{\xi}$ for a fixed run time τ. At the end of each run time, the particle tumbles instantaneously by selecting a new randomly chosen direction for the next run time. The amplitude of the motor force is $F_m = 1.0$ and the simulation time step is $\delta t = 0.002$, so in the absence of other forces a particle moves a distance called the run length $l_r = F_m \delta t \tau$ during each run time. To increase the activity of the particles, we increase τ while holding F_m fixed, so that the correlation time of the self-driven motion becomes larger. After applying the dc drive, we measure the time average of the velocity per particle for only the $\sigma_i = +1$ particles in the $+x$ dc drift direction, $\langle V\rangle = (2/N)\sum_{i=1}^{N}\delta(\sigma_i - 1)(\mathbf{v}_i \cdot \hat{\mathbf{x}})$, where $\mathbf{v}_i$ is the velocity of particle i. The corresponding average velocity in the drift direction curve for the $\sigma_i = -1$ particles is identical to $\langle V\rangle$ due to symmetry. We wait a minimum of 10^7 simulation time steps before taking the measurement to ensure that the system has reached a steady state. We select this particular form of particle-particle interaction since the dynamics of the laning transition for this effectively hard disk model in the nonactive limit has already been established [19]. This interaction model has been used extensively to study active matter clustering and phase separation [37,38,41,44]. We expect that similar results would arise under other forms of short-range interactions that are close to the hard sphere limit. It would be interesting in future studies to consider the effects of longer range repulsion such as Yukawa interactions or to introduce anisotropic interactions.

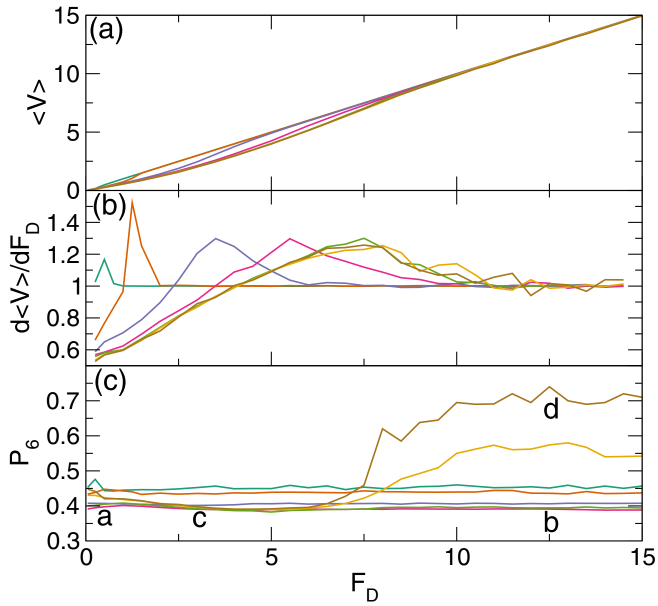

FIG. 1. (a) The average velocity per particle $\langle V\rangle$ in the dc drift direction for the $\sigma_i = +1$ particles vs F_D in a sample with particle density $\phi = 0.424$. The run-and-tumble particles have run time $\tau =$ 10 (teal), 30 (orange), 150 (periwinkle), 500 (pink), 2000 (green), 2×10^4 (gold), and 3.2×10^5 (brown). (b) The corresponding $d\langle V\rangle/dF_D$ vs F_D curves showing a peak that shifts to higher values of F_D as τ increases. (c) The corresponding fraction of sixfold-coordinated particles P_6 vs F_D. The $\tau = 2 \times 10^4$ and $\tau = 3.2 \times 10^5$ curves show a transition to a state with high triangular ordering, indicative of clustering. The letters **a**, **b**, **c**, and **d** mark the values of F_D at which the images in Fig. 2 were obtained.

III. LANING AND CLUSTERING AT LOW DENSITIES

Previous work on nonactive laning particles revealed that there are four dynamic phases: a jammed state (phase I), a fully phase separated state (phase II), a mixed or disordered state (phase III), and a laning state (phase IV) [19]. For particle densities $\phi < 0.55$, the system is always in a laning state, while for $\phi \geqslant 0.55$, the other three phases appear as well. For the active particles, we adopt the same nomenclature for phases I to IV, and define the low-density regime as $\phi < 0.55$. In Fig. 1(a), we plot $\langle V\rangle$ versus F_D for a sample with $\phi = 0.424$ for run lengths ranging from $\tau = 10$ to $\tau = 3.2 \times 10^5$. All of the velocity-force curves have nonlinear behavior at low drives

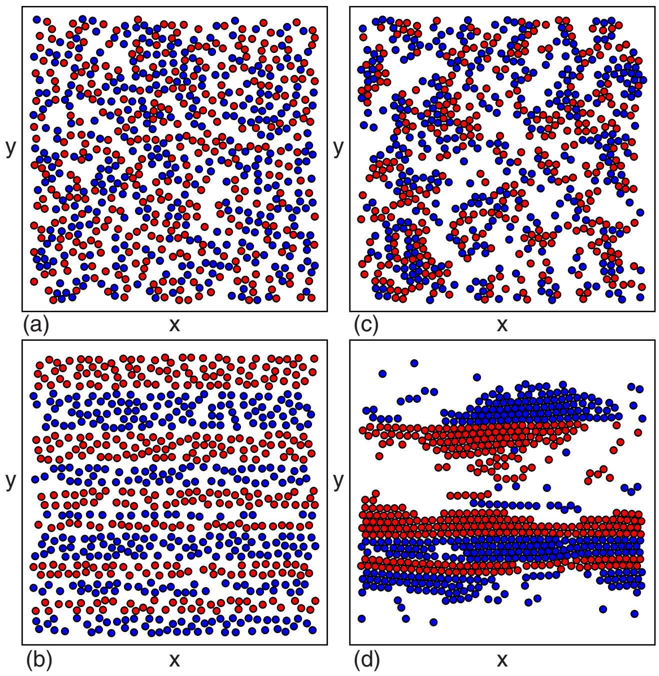

FIG. 2. Instantaneous positions of the $\sigma_i = +1$ (blue) and $\sigma_i = -1$ (red) run-and-tumble particles subjected to a drift force F_D. (a) A phase III mixed liquid state at $\tau = 500$ and $F_D = 0.5$. (b) A phase IV laning state at $\tau = 500$ and $F_D = 12.5$. (c) A phase III mixed state with local clustering at $\tau = 3.2 \times 10^5$ and $F_D = 3.0$. (d) A laning cluster phase V at $\tau = 3.2 \times 10^5$ and $F_D = 12.5$. The particles in the clusters have a significant amount of triangular ordering, producing an increase in P_6 in phase V in Fig. 1(c).

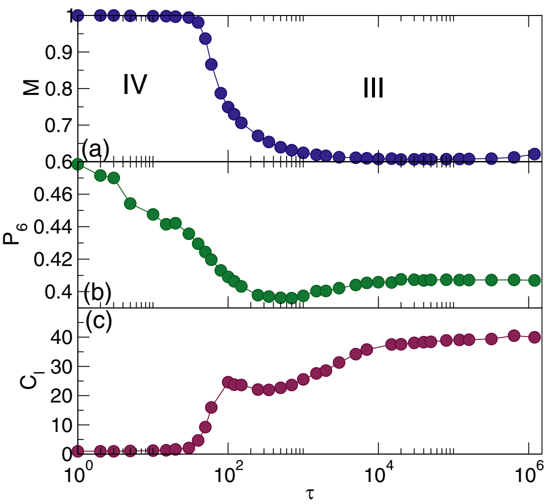

FIG. 3. (a) Mobility M vs τ for a system with $\phi = 0.424$ and $F_D = 2.0$. (b) The corresponding P_6 vs τ. (c) The corresponding average largest cluster size C_l vs τ. The IV-III transition that occurs with increasing τ is associated with a drop in M, a decrease in P_6, and an increase in C_l.

that transitions to a linear response at higher drives, as indicated by the peak in the $d\langle V\rangle/dF_D$ versus F_D curves in Fig. 1(b). The nonlinear behavior extends up to higher values of F_D as τ increases. For $\tau < 1.5 \times 10^4$, the peak in $d\langle V\rangle/dF_D$ coincides with the transition from disordered phase III flow to laning phase IV flow. Thus, as the activity is increased by raising τ, higher drift forces F_D must be applied in order to induce lane formation. In Fig. 2(a), we illustrate the particle positions at $\tau = 500$ and $F_D = 0.5$ in the phase III disordered or mixed liquid state, while in Fig. 2(b) we show the same system in phase IV at $F_D = 12.5$ where the particles form stable lanes.

In Fig. 1(c), we plot the fraction of sixfold-coordinated particles P_6 versus F_D. Here, $P_6 = N^{-1}\sum_{i=1}^{N}\delta(z_i - 6)$ where the coordination number z_i of particle i is obtained from a Voronoi construction. For $\tau < 1 \times 10^4$, there is no clear jump in P_6 at the transition from phase III to phase IV since, as shown in Fig. 2(b), the flowing lanes have no crystalline ordering. For $\tau > 1.5 \times 10^4$, phase IV is replaced by a new phase V, as indicated by the increase in P_6 at large F_D for the $\tau = 2 \times 10^4$ and $\tau = 3.2 \times 10^5$ curves. Phase V is what we term a clustered laning state, as illustrated in Fig. 2(d) at $\tau = 3.2 \times 10^5$ and $F_D = 12.5$. Here the particles form clusters similar to the activity-induced clusters that appear in an undriven active matter system [32–38], but within each cluster, phase segregation into the two oppositely moving particle species occurs in order to eliminate particle-particle collisions. Triangular ordering of the particles emerges within the denser clusters, leading to the increase in P_6 at the onset of phase V.

For the same large $\tau = 3.2 \times 10^5$ at a lower drive of $F_D = 3.0$, a phase III disordered mixed phase occurs as illustrated in Fig. 2(c), where a small amount of clustering is visible due to the high activity level.

We define the mobility $M = \langle V\rangle/V_0$ as the average particle velocity divided by the expected free flow velocity $V_0 = F_D/\eta$ of an individual particle in the absence of particle-particle interactions. In Fig. 3(a), we plot M versus τ for a system with $\phi = 0.424$ at $F_D = 2.0$, where $V_0 = 2.0$. For $\tau < 100$, the system forms a phase IV laning state similar to that illustrated in Fig. 2(b), and as τ increases, a transition to phase III occurs that is accompanied by a sharp decrease in the mobility from $M = 1.0$ to $M = 0.62$. The corresponding P_6 versus F_D curve appears in Fig. 3(b), showing that P_6 decreases with increasing τ but has no sharp feature at the IV-III transition. In Fig. 3(c), we plot C_l, the average largest cluster size, versus τ for the same system. To measure C_l, we group the particles into clusters by identifying all particles that are in direct contact with each other, determine the number of particles N_c^j in a given cluster j, and obtain $C_l = \langle \max\{N_c^j\}_{i=1}^N\rangle$ where the average is taken over a series of simulation time steps. Larger values of C_l indicate that particle-particle collisions are more frequent. In steady-state phase IV flow, the particles only experience brief pairwise collisions, so $C_l < 3$; additionally, the mobility is close to $M = 1$ since the particles are undergoing nearly free flow. At the IV-III transition, the particle collision frequency increases, lowering the mobility, while the cluster size increases, with C_l reaching values of 30 or more. The IV-III transition that occurs when τ increases can be regarded as analogous to a transition in a social system from orderly laning flows of noncolliding pedestrians to a panic state in which pedestrians collide and impede each other's flow. Here, the run time would correspond to an agitation level which, above a certain threshold, destroys the orderly flow and produces a low mobility collisional flow. There is a small decrease in C_l near $\tau = 102$ that is correlated with the minimum in P_6. In this regime, τ is just large enough

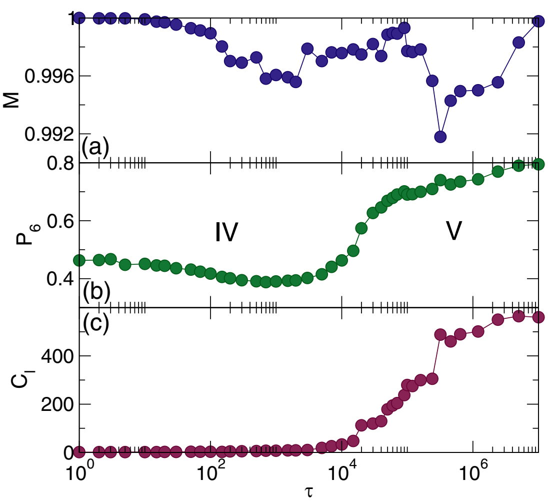

FIG. 4. (a) Mobility M vs τ for a system with $\phi = 0.424$ at $F_D = 12.5$. (b) The corresponding P_6 vs τ. (c) The corresponding average largest cluster size C_l vs τ. At the IV-V transition, both P_6 and C_l increase, but there is little change in M.

for a cluster state to form. When τ increases slightly, the clusters become sufficiently long-lived to generate collisions that reduce the flow velocity, but these collisions cause the cluster size to decrease. At larger τ, the clusters are more robust and C_l increases again.

In Figs. 4(a)–4(c), we plot M, P_6, and C_l versus τ for the $\phi = 0.424$ system from Fig. 3 at a higher drive of $F_D = 12.5$, where very different behavior appears. At low τ, the system is initially in the phase IV laning state due to the large drive, and as τ increases, a transition occurs into the clustered laning phase V illustrated in Fig. 2(d), rather than the disordered phase III flow that appears at lower F_D. In phase IV, C_l is low since particle collisions are rare, and $P_6 \approx 0.5$ due to the one-dimensional liquid structure of the flow. At the transition to phase V, both C_l and P_6 increase to $C_l \approx 500$ and $P_6 \approx 0.8$, while there is very little change in the mobility M. Unlike the mixed flow found in phase III, phase V is is mostly phase separated as shown in Fig. 2(d), so the mobility is high even though C_l is large, since the particle-particle interactions are dominated by static contacts within the moving clusters rather than by collisional contacts between clusters moving in opposite directions.

In Fig. 5, we construct a dynamic phase diagram as a function of F_D versus τ for a system with $\phi = 0.424$, highlighting the regimes of phase III, IV, and V flow. The transitions between the phases are identified based on changes in M, P_6, and C_l. For $F_D < 8.0$, the system is in phase IV at small τ and phase III at large τ, as illustrated in Fig. 3. For $0 < \tau < 1.5 \times 10^4$, the IV-III transition line shifts to larger F_D with increasing τ. For $\tau > 1.5 \times 10^5$ and $F_D > 8.0$, the system is still in phase IV at small τ but is in phase V at large τ, as shown in Fig. 4. We note that at this particle density of $\phi = 0.424$, when $F_D = 0$ there is no activity-induced clustered state, since as shown in previous studies of this model in a similar regime, such a state arises only for $\phi > 0.45$ [19]. The results in Fig. 5 indicate that driving can induce the formation of a clustered state at large activity even at particle densities for which activity alone cannot produce a clustered state. This

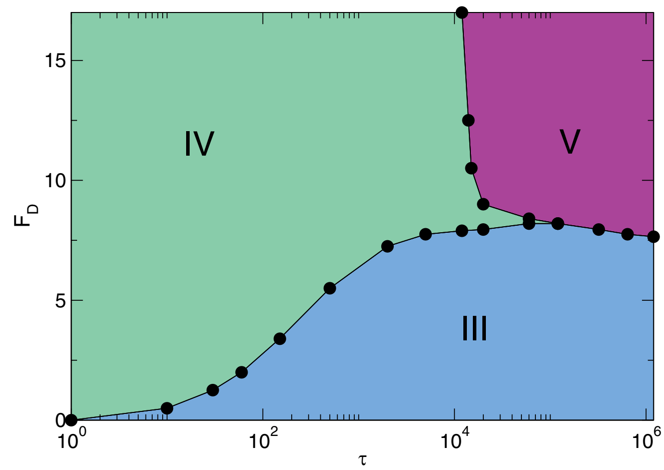

FIG. 5. Dynamic phase diagram as a function of F_D vs τ at $\phi = 0.424$. Phase III, disordered mixing flow state; phase IV, laning state; and phase V, clustered laning state.

suggests that active nonclustering fluid states could transition to a clustered state under application of a shear or other external driving. We note that shearing could have a different effect from the driving applied in this work, since it is possible that the shear could break apart the clusters more effectively.

IV. DRIVE-INDUCED ACTIVE PHASE SEPARATION

We next study the evolution of phases IV and V in greater detail over a range of particle densities and external drives. In Fig. 6, we plot P_6 versus F_D at $\tau = 3.2 \times 10^5$ for particle densities ranging from $\phi = 0.06$ to $\phi = 0.848$. At the lowest values of F_D, when $\phi < 0.475$, $P_6 < 0.45$ and the system is always in a disordered state as illustrated in Fig. 7(a) at $\phi = 0.182$ and $F_D = 0.01$. When $\phi > 0.4$, there is a transition to a cluster state in the absence of drive, and this cluster state, which we term phase CL, persists at low drives, as shown in Fig. 7(b) for $\phi = 0.6$ and $F_d = 0.01$. Here, a dense, solidlike

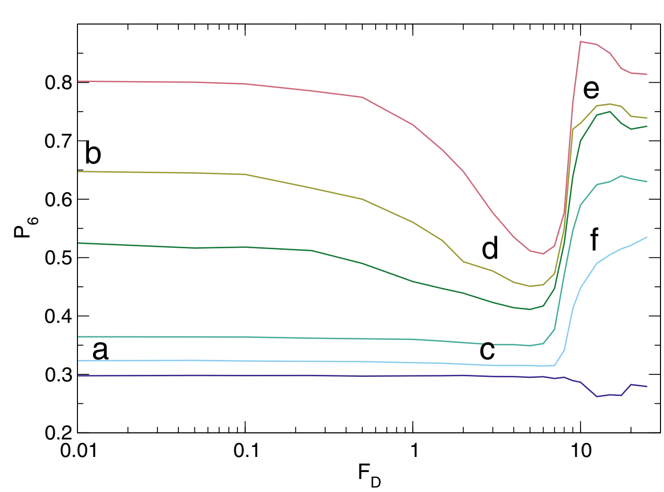

FIG. 6. P_6 vs F_D at $\tau = 3.2 \times 10^5$ for $\phi = 0.06$, 0.182, 0.303, 0.48, 0.6, and 0.848, from bottom to top. The letters **a** to **f** indicate the points at which the images in Fig. 7 were obtained.

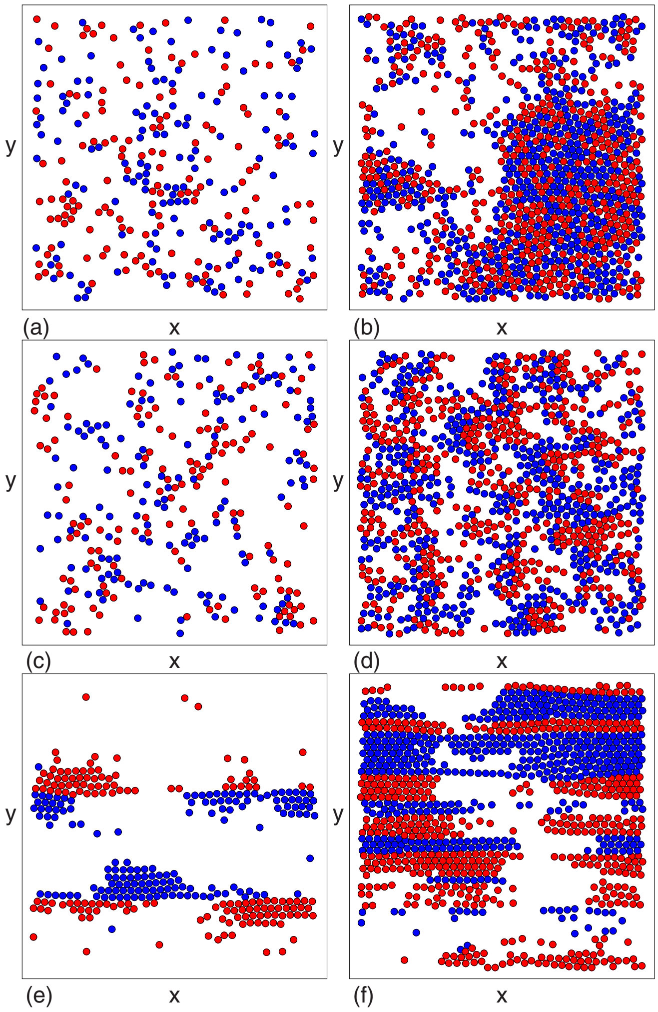

FIG. 7. Instantaneous positions of the $\sigma_i = +1$ (blue) and $\sigma_i = -1$ (red) run-and-tumble particles from the system in Fig. 6 at $\tau = 3.2 \times 10^5$. (a) Phase III at $\phi = 0.182$ and $F_D = 0.01$. (b) At $\phi = 0.6$ and $F_D = 0.01$, a cluster state forms with no separation of the different species. We call this phase CL. (c) Phase III at $\phi = 0.182$ and $F_D = 3.0$. (d) Phase III with weak clustering at $\phi = 0.6$ and $F_D = 3.0$. (e) Phase V, the laning cluster state, at $\phi = 0.182$ and $F_D = 12.5$. (f) Phase V at $\phi = 0.6$ at $F_D = 12.5$.

region with a significant amount of triangular ordering is surrounded by a low-density liquid. The cluster state has a density phase separation into high- and low-density regions; however, there is no segregation of the two particle species, which distinguishes phase CL from the laning cluster phase V. At intermediate values of F_D, the disordered flow phase III appears as shown in Fig. 7(c) for $\phi = 0.182$ and $F_D = 3.0$. The larger F_D value tears apart the cluster state for $\phi > 0.4$, producing in its place a disordered phase III flow with some residual clustering, as illustrated in Fig. 7(d) at $\phi = 0.6$ and $F_D = 3.0$. In Figs. 7(e) and 7(f), we show the $F_D = 12.5$ states at $\phi = 0.182$ and $\phi = 0.6$, respectively. In both cases, a laning cluster phase V appears, producing the higher values of P_6 found in Fig. 6. Phase V persists all the way down to $\phi = 0.06$ for this high drive; however, at the smaller values of ϕ the phase-separated regions become more one-dimensional in nature, so P_6 remains low because of the smaller coordination

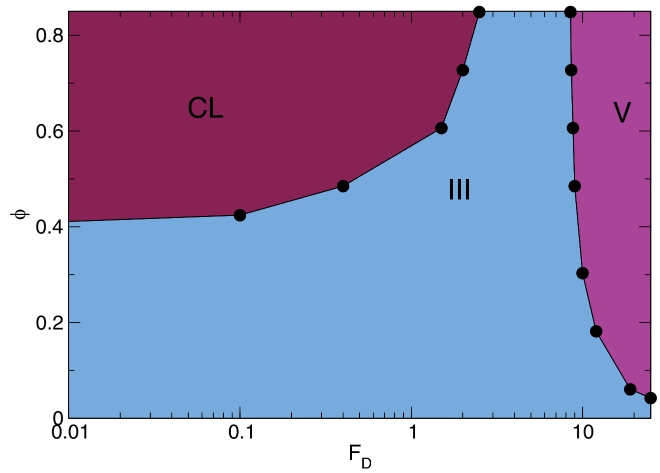

FIG. 8. Dynamic phase diagram as a function of ϕ vs F_D for the system in Figs. 6 and 7 at $\tau = 3.2 \times 10^5$. At small F_D, there is a transition from phase III to a cluster state CL with increasing ϕ, while large drives can produce phase V.

number of the particles in these chainlike structures. Based on the features in Fig. 7 along with additional simulation data, we construct a dynamic phase diagram as a function of ϕ versus F_D for $\tau = 3.2 \times 10^5$ as shown in Fig. 8. This result suggests that the introduction of driving can break up the clusters that form due to activity-induced density segregation; however, for sufficiently large driving, a new type of clustering instability can arise. Application of a shear instead of a dc drive could produce effects different than what we find here.

In Fig. 9, we plot a dynamic phase diagram as a function of F_D vs ϕ for a small run time of $\tau = 500$. In this case, neither phase CL nor phase V appear. In Fig. 10(a), we illustrate the instantaneous particle configuration in the laning phase IV for the system in Fig. 9 at $F_D = 12.5$, $\phi = 0.848$, and $\tau = 500$, At the same values of F_D and ϕ but at $\tau = 3.2 \times 10^5$ as in Fig. 8, Fig. 10(b) shows that the system forms a laning clustered state containing low-density regions. At $F_D = 12.5$ and $\phi = 0.303$, Fig. 10(c) indicates that the $\tau = 500$ system from Fig. 9

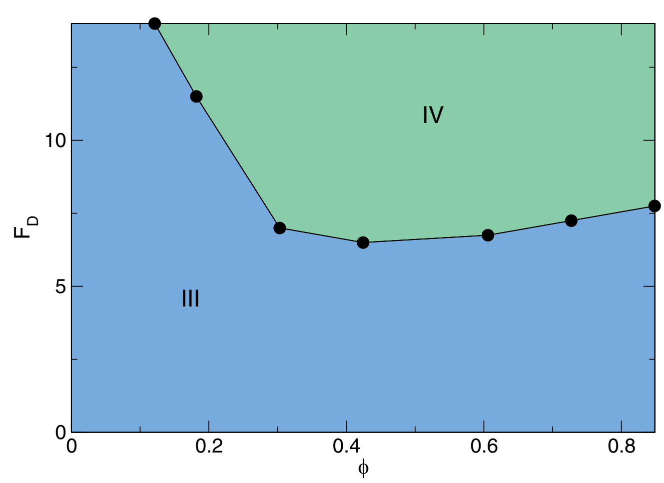

FIG. 9. Dynamic phase diagram as a function of ϕ vs F_D at $\tau = 500$ showing phases III and IV.

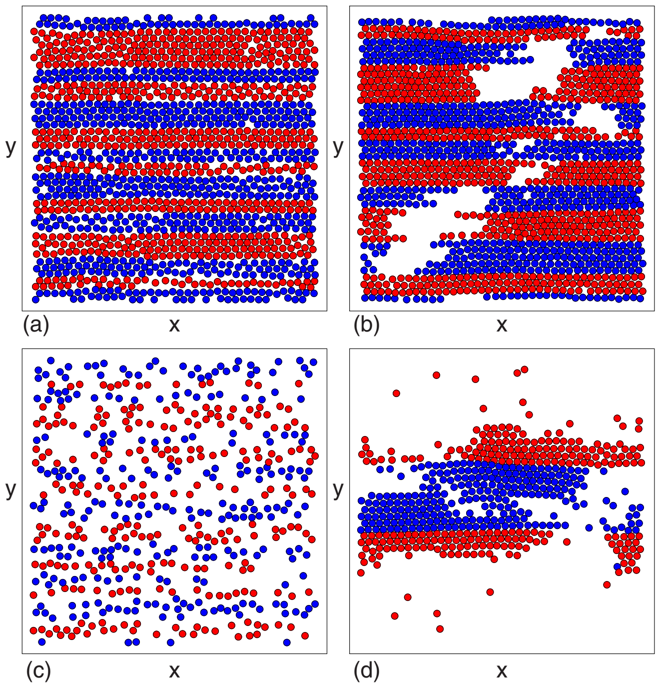

FIG. 10. A comparison of the instantaneous particle configurations of the $\sigma_i = +1$ (blue) and $\sigma_i = -1$ (red) run-and-tumble particles for the systems in Figs. 8 and 9 at $F_D = 12.5$. [(a), (b)] $\phi = 0.848$: (a) The laning phase IV for the system in Fig. 9 with $\tau = 500$. (b) The laning clustered phase V for the system in Fig. 8 with $\tau = 3.2 \times 10^5$. [(c), (d)] $\phi = 0.303$: (c) A laning phase IV without triangular ordering for the system in Fig. 9 with $\tau = 500$. (d) The laning clustered phase V for the system in Fig. 8 with $\tau = 3.2 \times 10^5$.

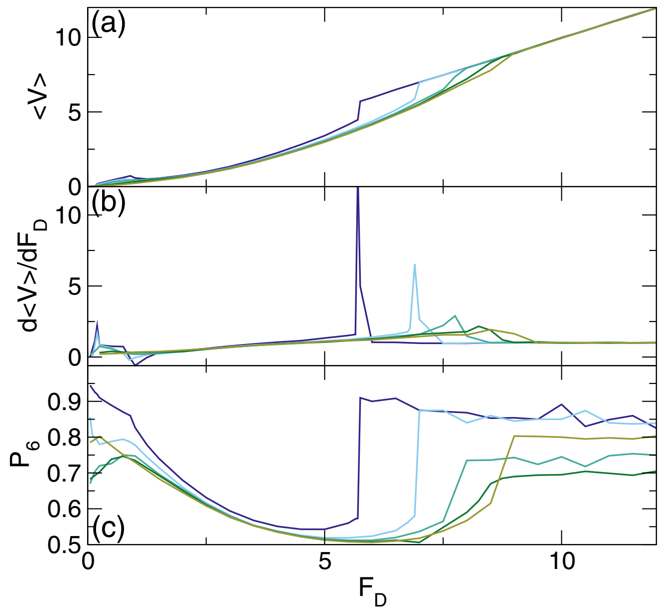

FIG. 11. A system at $\phi = 0.848$ with $\tau = 10$ (dark blue), 150 (light blue), 500 (light green), 2000 (dark green), and 2×10^4 (gold). (a) $\langle V \rangle$ vs F_D. (b) $d\langle V \rangle/dF_D$ vs F_D. (c) P_6 vs F_D. For $\tau < 500$, we observe phase I (jammed), II (phase separated), III (disordered mixed flow), and IV (laning flow). Transitions between these phases appear as features in $d\langle V \rangle/dF_D$: an initial spike near $F_D = 0.15$ is the I-II transition, a negative region near $F_D = 1.0$ is the II-III transition, and the large spike that appears for $F_D > 5.0$ is the III-IV transition. For $\tau > 1.5 \times 10^4$, the III-IV transition is replaced by a III-V transition.

enters a phase IV flow with no triangular ordering, while in Fig. 10(d), the $\tau = 3.2 \times 10^5$ system from Fig. 8 forms the laning clustered phase V.

This system could also serve as a soft matter realization of certain types of social dynamics such as pedestrian flows and could be used to study the transition from orderly laning flow to disordered or panic motion. In this context, if phase III is identified as disorderly pedestrian flow and phase IV as orderly flow, then our main conclusion would be that the activity timescale strongly influences the force required to approach the transition, as in Fig. 5, while further increasing an already large pedestrian density may not be such a significant factor, as in Fig. 9.

We note that the clustering transition which we observe has both similarities and differences from the motility-induced phase separation found in active matter systems without external driving. In each case, clustering occurs only when the activity is high enough; however, the clustering transition disappears at lower densities in the nondriven system [33,37], whereas in the driven system, the clustering can persist to very low densities.

V. DENSE PHASE

We next consider the role of activity in the dense phase with $\phi = 0.848$. Here, when $F_D < 1.0$, we find two additional phases: a jammed state (phase I) and a phase-separated state (phase II). In Fig. 11(a), we plot representative $\langle V \rangle$ versus F_D curves for run times ranging from $\tau = 10$ to $\tau = 2 \times 10^4$. Figure 11(b) shows the corresponding $d\langle V \rangle/dF_D$ versus F_D curves and in Fig. 11(c) we plot P_6 versus F_D. For $\tau < 500$, we find the jammed phase I in which $\langle V \rangle = 0$ and $d\langle V \rangle/dF_D = 0$. The particle configurations in the two variations of the jammed state are illustrated in Figs. 12(a) and 12(b) for $\tau = 10$ at $F_D = 0.01$ and $F_D = 0.15$, respectively. When $F_D < 0.05$, the system remains in its initially deposited configuration and only small rearrangements occur before the particles settle into a motionless jammed state, while for $F_D > 0.05$, the system undergoes transient large-scale rearrangements before organizing into a jammed state of the type illustrated in Fig. 12(b). Here there is both a density phase separation into high- and zero-density regions as well as a species phase separation, with the $\sigma_i = -1$ particles preferentially sitting to the left of the $\sigma_i = +1$ particles and blocking their motion. In phase II, the phase-separated state illustrated in Fig. 12(c) for $F_D = 0.5$, each particle species forms a mostly triangular solid, giving a large value of P_6. The I-II transition is associated with a spike in the $d\langle V \rangle/dF_D$ curves near $F_D = 0.15$. Within phase II, the phase separation allows the particles to move without collisions, so individual particles move at nearly the free flow velocity V_0 and the mobility $M \approx 1$. As F_D increases, a II-III transition occurs. We illustrate the disordered mixed flow phase III in Fig. 12(d) for $\tau = 10$ and $F_D = 1.5$. The particles are in a fluctuating state and undergo numerous collisions, reducing the mobility. Just above the transition into phase III, some clustering of the particles persists, as shown in

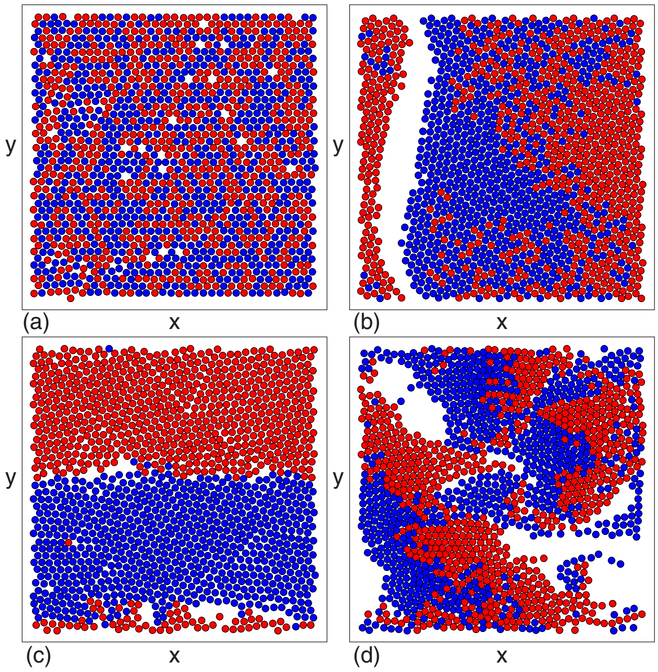

FIG. 12. Instantaneous positions of the $\sigma_i = +1$ (blue) and $\sigma_i = -1$ (red) run-and-tumble particles in the system from Fig. 11 with $\phi = 0.848$ and $\tau = 10$. (a) The jammed phase I at $F_D = 0.01$. (b) The jammed phase I at $F_D = 0.15$. (c) The phase-separated state (phase II) at $F_D = 0.5$. (d) The disordered mixed flow phase III at $F_D = 1.5$.

Fig. 12(d). As F_D increases, the size of these clusters drops, causing P_6 to decline. The II-III transition is associated with a drop in $\langle V\rangle$ and P_6 along with negative values of $d\langle V\rangle/dF_D$, indicative of negative differential conductivity. For $F_D > 5.0$ and $\tau < 1.5 \times 10^4$, the system transitions from phase III to the laning cluster phase IV as shown previously, and this transition corresponds with upward jumps in $\langle V\rangle$ and P_6 and a large positive spike in $d\langle V\rangle/dF_D$. For $\tau > 500$, phases I and II disappear, as indicated by the loss of the spikes in $d\langle V\rangle/dF_D$ and the reduced value of P_6 at small values of F_D. The III-IV transition shifts to higher values of F_D as τ increases, as shown by the shift in the $d\langle V\rangle/dF_D$ peak in Fig. 11(b). In phase IV, P_6 gradually decreases with increasing τ up to $\tau = 1 \times 10^4$, after which P_6 begins to increase again when phase IV is replaced by phase V as shown previously. The transition to phase V is marked by a weak local maximum in $d\langle V\rangle/dF_D$.

We can characterize the dynamics of the dense phase in terms of three driving force regimes. At small drives, $F_D < 1.25$, phases I and II appear. For intermediate values, $1.25 < F_D < 5.5$, the system is predominately in phase III. At high drives of $F_D > 5.5$, phases IV and V occur.

In Fig. 13(a), we plot $\langle V\rangle$ versus τ for a system with $\phi = 0.848$ and $F_D = 0.15$, and we show the corresponding P_6 versus F_D curve in Fig. 13(b). For $\tau < 20$, the system always forms a jammed phase I state with $\langle V\rangle = 0.0$ and a high value of P_6. Previous work with $\tau = 0$ showed that phase II followed phase I upon increasing F_D [19], while in Fig. 13 with fixed F_D, phase II occurs for $20 < \tau < 60$ as indicated by the high value of $\langle V\rangle$ in this regime. We find that when $60 < \tau < 300$, the system can organize into either the jammed phase I or the phase-separated state (phase II) as shown by the jumps in $\langle V\rangle$

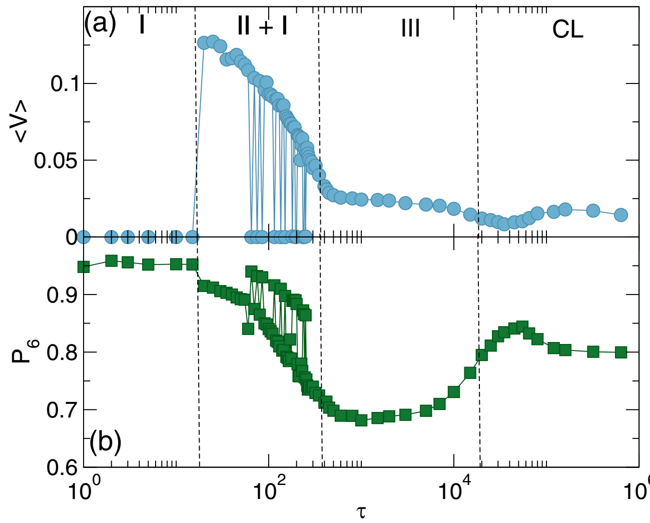

FIG. 13. (a) $\langle V\rangle$ vs τ at $F_D = 0.15$ and $\phi = 0.848$. (b) The corresponding P_6 vs τ. The system always reaches phase I for $\tau < 20$ and phase II for $20 < \tau < 65$, while for $65 < \tau < 300$ the system can settle into either phase I or phase II. At larger τ, phase III flow is stable, and for $\tau > 1.5 \times 10^4$, phase CL flow occurs.

between $\langle V\rangle = 0$ and $\langle V\rangle \approx V_0$, the free flow velocity. The plot in Fig. 13 was obtained from individual realizations for each value of τ; however, if we average the value of $\langle V\rangle$ over many different realizations for each τ, we obtain $\langle\tilde{V}\rangle = 0.05$ in this fluctuating regime since the system is in phase I for half of the realizations and in phase II for the other half. The reentrant behavior of phase I arises due to an effect similar to freezing by heating [2], since the increase in the run time makes the particle act as if it had an effectively larger radius, making the system susceptible to jamming. In Fig. 14, we show the particle positions and trajectories in the reentrant phase I for $\tau = 200$. Here the jammed phase takes the form of a triangular lattice, while in the low-density region, the particles are moving in a liquid-like fashion. The appearance of the mixed phase I + phase II regime is probably strongly size dependent, similar to the observation that the freezing by heating phenomenon is enhanced by confinement [2]. For $\tau > 300$ in Fig. 13, the activity is large enough to break apart the crystalline structure of phase I and the system enters the disordered mixing phase III, which coincides with a dip in P_6 and a drop in $\langle V\rangle$. For $\tau > 1.5 \times 10^4$, an increase in P_6 coincides with the onset of the activity-included clustering phase CL in which $\langle V\rangle$ remains low. We find similar behavior as a function of τ over the range $0 < F_D < 0.2$, with the extent of the jammed phase I increasing as F_D decreases.

In Figs. 15(a) and 15(b), we show $\langle V\rangle$ and P_6 versus τ for samples with $\phi = 0.848$ at $F_D = 1.5$, where the system is always in phase III. Here $\langle V\rangle$ gradually decreases from $\langle V\rangle = 0.575$ at $\tau = 1.0$ to $\langle V\rangle = 0.47$ with increasing τ, while P_6 decreases from $P_6 = 0.74$ to $P_6 = 0.69$. We find similar behavior for higher F_D up to $F_D = 5.5$.

In Fig. 16, we plot $\langle V\rangle$ and P_6 versus τ at $F_D = 6.5$ and $\phi = 0.848$ where the system is in the laning phase IV up to $\tau = 100$. Within phase IV, $\langle V\rangle \approx 6.5$ and $P_6 \approx 0.9$. At the transition to phase III, there is an abrupt drop in both $\langle V\rangle$

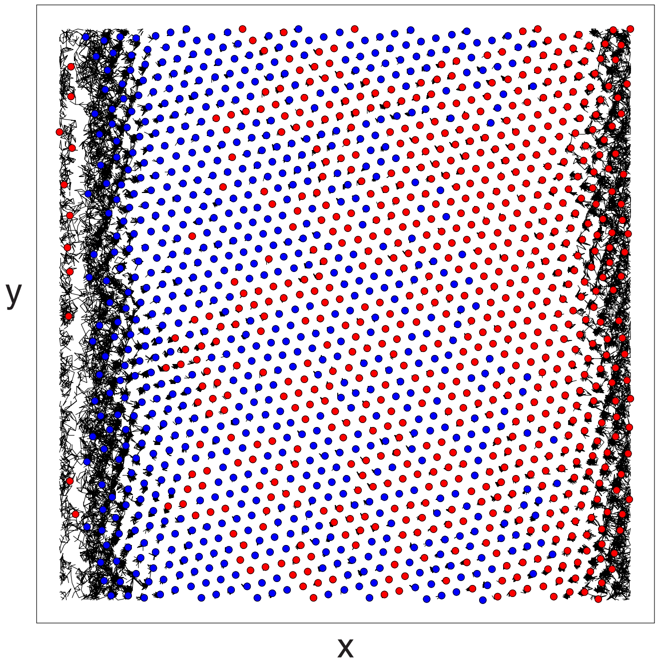

FIG. 14. Trajectories over a fixed time period (lines) and instantaneous particle positions of the $\sigma_i = +1$ (blue circles) and $\sigma_i = -1$ (red circles) run-and-tumble particles for the system in Fig. 13 at $\tau = 200$ and $\phi = 0.848$, which reaches a reentrant jammed phase I. For clarity, in this image we have reduced the radii of the circles representing the particles in order to make the trajectories visible. Here there is a coexistence of a jammed state with a liquid.

and P_6 when the onset of collisions between the two species decreases the flow. In Figs. 17(c) and 17(d), we show $\langle V \rangle$ and P_6 versus τ in the same system at $F_D = 12.5$ where a IV-V transition occurs near $\tau = 1.5 \times 10^4$. At the transition, a dip in P_6 appears but there is little change in $\langle V \rangle$. By conducting a series of simulations and examining the features in P_6 and $\langle V \rangle$ along with images of the particle configurations, we construct a dynamic phase diagram as a function of F_D versus τ for the

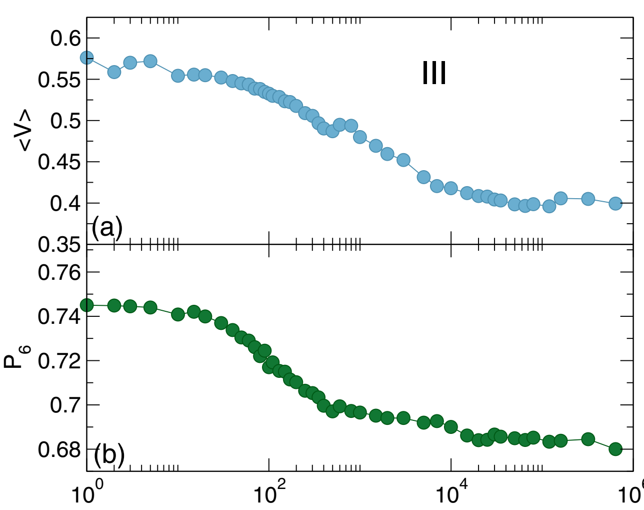

FIG. 15. (a) $\langle V \rangle$ vs τ at $F_D = 1.5$ and $\phi = 0.848$ where the system is always in phase III. (b) The corresponding P_6 vs τ.

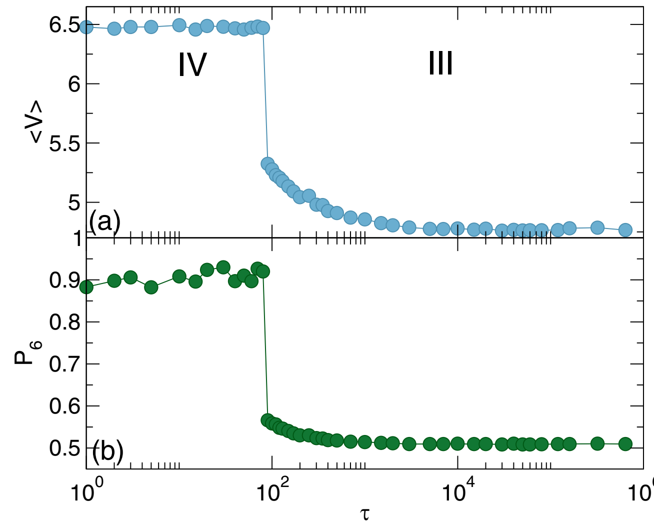

FIG. 16. (a) $\langle V \rangle$ vs τ at $F_D = 6.5$ and $\phi = 0.848$. (b) The corresponding P_6 vs τ. Here the system undergoes a IV-III transition.

$\phi = 0.848$ system, as shown in Fig. 18. In the region marked phase I, the system always reaches a jammed state, while in the region marked phase II, the system is either in steady-state phase II flow or falls into a re-entrant phase I jammed state. Phases I and II appear only when $\tau < 500$. Phase IV occurs at large F_D when $\tau < 15\,000$, phase CL occurs only when $\tau > 15\,000$, and phase III separates phase II from phase IV, phase II from phase CL, and phase CL from phase V.

The phases we observe are robust for different system sizes. The transient times to reach the different phases increase with increasing system size, but there is little change in the locations of the phase transitions. The fluctuations in our system are produced by the activity; however, if an additional noise term such as a white noise is added, the phases remain stable until the noise becomes large enough to disorder the flow. Such an effect is akin to adding thermally induced fluctuations, where the

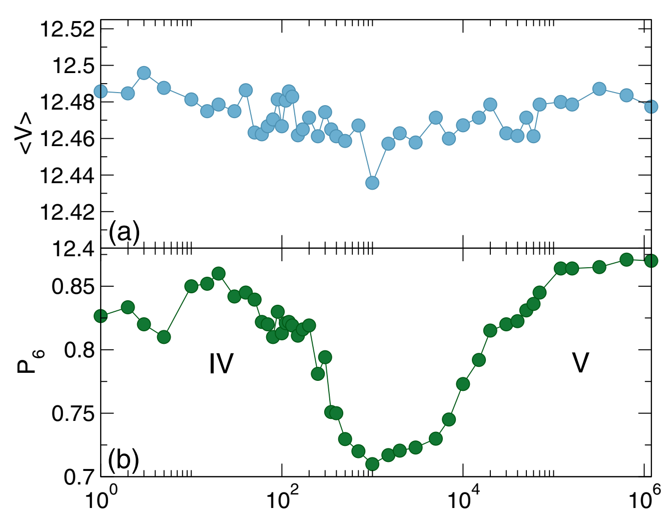

FIG. 17. (a) $\langle V \rangle$ vs τ at $F_D = 12.5$ and $\phi = 0.848$. (b) The corresponding P_6 vs τ. The IV-V transition appears as a dip in P_6, but there is is little change in $\langle V \rangle$ across the transition.

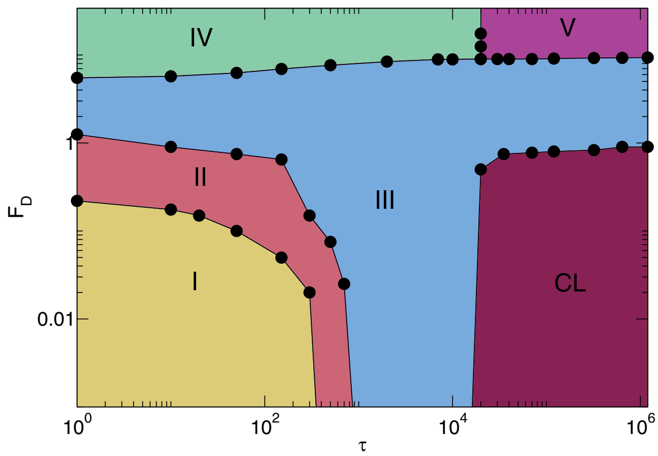

FIG. 18. Dynamic phase diagram as a function of F_D vs τ at $\phi = 0.848$. In the region marked I, the system always reaches the jammed phase I, while in the region marked II, the system sometimes reaches steady-state phase II flow and sometimes enters a re-entrant jammed phase I. Phase III is disordered mixing flow, phase IV is a laning state, phase V consists of laning cluster motion, and CL is the cluster phase.

system disorders at high temperatures, but the phases remain stable over a range of lower temperatures. In this case, the noise would cause the locations of the transitions to shift. For example, in Fig. 18, phase III would gradually grow as the noise fluctuations increase.

VI. SUMMARY

We have examined a two-dimensional binary system of particles driven in opposite directions where we introduce particle self-propulsion in the form of run-and-tumble dynamics. Previous work on this system in the nonactive limit revealed four dynamic phases: jammed, phase separated, disordered mixing flow, and laning flow. At low particle densities, the nonactive system exhibits both laning and disordered flow phases. As the activity is increased, the laning phase transitions into a disordered flow phase as indicated by both a drop in the average mobility and an increase in the frequency of particle-particle collisions. The transition also appears as a clear change in the velocity-force curve constructed using the average velocity of one particle species as a function of the external drift force. In terms of social systems, such a transition can be compared to a change from an orderly high-mobility flow of agents such as pedestrians to a low-mobility panic state in which the agents collide. At high drives, we find a novel laning cluster state in which the particles undergo both density phase segregation and species phase segregation. The laning cluster state remains stable well below the density at which an activity-induced cluster state forms in an undriven system. This suggests that an externally applied drive can serve as an alternative method of inducing cluster formation in an active system. At high particle densities, we find a total of six dynamic phases, including the jammed, phase separated, laning, and disordered flows, the laning cluster state, and an activity-induced cluster state which appears for small external drift forces. The activity can induce formation of a partially reentrant jammed state at low drift forces through a freezing by heating mechanism. Our results show that binary driven active particles exhibit a rich variety of behaviors. There are already several nonactive experimental systems that can be modeled as binary driven systems, and it may be possible to realize variations of active matter binary driven systems that would exhibit the behavior we describe.

ACKNOWLEDGMENTS

We gratefully acknowledge the support of the U.S. Department of Energy through the LANL/LDRD program for this work. This work was carried out under the auspices of the NNSA of the U.S. DoE at LANL under Contract No. DE-AC52-06NA25396 and through the LANL/LDRD program.

[1] B. Schmittmann and R. K. P. Zia, Driven diffusive systems: An introduction and recent developments, Phys. Rep. **301**, 45 (1998).
[2] D. Helbing, I. J. Farkas, and T. Vicsek, Freezing by Heating in a Driven Mesoscopic System, Phys. Rev. Lett. **84**, 1240 (2000).
[3] J. Dzubiella, G. P. Hoffmann, and H. Löwen, Lane formation in colloidal mixtures driven by an external field, Phys. Rev. E **65**, 021402 (2002).
[4] R. R. Netz, Conduction and diffusion in two-dimensional electrolytes, Europhys. Lett. **63**, 616 (2003).
[5] J. Chakrabarti, J. Dzubiella, and H. Löwen, Reentrance effect in the lane formation of driven colloids, Phys. Rev. E **70**, 012401 (2004).
[6] T. Glanz and H. Löwen, The nature of the laning transition in two dimensions, J. Phys.: Condens. Matter **24**, 464114 (2012).
[7] K. Klymko, P. L. Geissler, and S. Whitelam, Origin and macroscopic implications of lane formation in mixtures of oppositely driven particles, Phys. Rev. E **94**, 022608 (2016).
[8] A. Poncet, O. Bénichou, V. Démery, and G. Oshanin, Universal Long Ranged Correlations in Driven Binary Mixtures, Phys. Rev. Lett. **118**, 118002 (2017).
[9] M. E. Leunissen, C. G. Christova, A.-P. Hynninen, C. P. Royall, A. I. Campbell, A. Imhof, M. Dijkstra, R. van Roij, and A. van Blaaderen, Ionic colloidal crystals of oppositely charged particles, Nature (London) **437**, 235 (2005).
[10] T. Vissers, A. Wysocki, M. Rex, H. Löwen, C. P. Royall, A. Imhof, and A. van Blaaderen, Lane formation in driven mixtures of oppositely charged colloids, Soft Matter **7**, 2352 (2011).
[11] T. Vissers, A. van Blaaderen, and A. Imhof, Band Formation in Mixtures of Oppositely Charged Colloids Driven by an ac Electric Field, Phys. Rev. Lett. **106**, 228303 (2011).
[12] K. R. Sütterlin, A. Wysocki, A. V. Ivlev, C. Räth, H. M. Thomas, M. Rubin-Zuzic, W. J. Goedheer, V. E. Fortov, A. M. Lipaev, V. I. Molotkov, O. F. Petrov, G. E. Morfill, and H. Löwen, Dynamics of Lane Formation in Driven Binary Complex Plasmas, Phys. Rev. Lett. **102**, 085003 (2009).

[13] C.-R. Du, K. R. Sütterlin, A. V. Ivlev, H. M. Thomas, and G. E. Morfill, Model experiment for studying lane formation in binary complex plasmas, Europhys. Lett. **99**, 45001 (2012).
[14] M. Moussaid, S. Garnier, G. Theraulaz, and D. Helbing, Collective information processing and pattern formation in swarms, flocks, and crowds, Topics Cognitive Sci. **1**, 469 (2009).
[15] I. D. Couzin and N. R. Franks, Self-organized lane formation and optimized traffic flow in army ants, Proc. Roy. Soc. B **270**, 139 (2003).
[16] H. Ohta, Lane formation in a lattice model for oppositely driven binary particles, Europhys. Lett. **99**, 40006 (2012).
[17] T. Glanz, R. Wittkowski, and H. Löwen, Symmetry breaking in clogging for oppositely driven particles, Phys. Rev. E **94**, 052606 (2016).
[18] K. Ikeda and K. Kim, Lane formation dynamics of oppositely self-driven binary particles: Effects of density and finite system size, J. Phys. Soc. Jpn. **86**, 044004 (2017).
[19] C. Reichhardt and C. J. O. Reichhardt, Velocity force curves, laning, and jamming for oppositely driven disk systems, Soft Matter **14**, 490 (2018).
[20] C. Reichhardt and C. J. O. Reichhardt, Cooperative behavior and pattern formation in mixtures of driven and nondriven colloidal assemblies, Phys. Rev. E **74**, 011403 (2006).
[21] C. Reichhardt and C. J. O. Reichhardt, Stripes, clusters, and nonequilibrium ordering for bidisperse colloids with repulsive interactions, Phys. Rev. E **75**, 040402 (2007).
[22] A. Wysocki and H. Löwen, Oscillatory driven colloidal binary mixtures: Axial segregation versus laning, Phys. Rev. E **79**, 041408 (2009).
[23] M. Ikeda, H. Wada, and H. Hayakawa, Instabilities and turbulence-like dynamics in an oppositely driven binary particle mixture, Europhys. Lett. **99**, 68005 (2012).
[24] B. Heinze, U. Siems, and P. Nielaba, Segregation of oppositely driven colloidal particles in hard-walled channels: A finite-size study, Phys. Rev. E **92**, 012323 (2015).
[25] C. W. Wächtler, F. Kogler, and S. H. L. Klapp, Lane formation in a driven attractive fluid, Phys. Rev. E **94**, 052603 (2016).
[26] M. C. Cross and P. C. Hohenberg, Pattern formation outside of equilibrium, Rev. Mod. Phys. **65**, 851 (1993).
[27] T. Mullin, Coarsening of Self-Organized Clusters in Binary Mixtures of Particles, Phys. Rev. Lett. **84**, 4741 (2000).
[28] P. Sánchez, M. R. Swift, and P. J. King, Stripe Formation in Granular Mixtures Due to the Differential Influence of Drag, Phys. Rev. Lett. **93**, 184302 (2004).
[29] C. Lozano, I. Zuriguel, A. Garcimartín, and T. Mullin, Granular Segregation Driven by Particle Interactions, Phys. Rev. Lett. **114**, 178002 (2015).
[30] M. C. Marchetti, J. F. Joanny, S. Ramaswamy, T. B. Liverpool, J. Prost, M. Rao, and R. A. Simha, Hydrodynamics of soft active matter, Rev. Mod. Phys. **85**, 1143 (2013).
[31] C. Bechinger, R. Di Leonardo, H. Löwen, C. Reichhardt, G. Volpe, and G. Volpe, Active Brownian particles in complex and crowded environments, Rev. Mod. Phys. **88**, 045006 (2016).
[32] Y. Fily and M. C. Marchetti, Athermal Phase Separation of Self-Propelled Particles with No Alignment, Phys. Rev. Lett. **108**, 235702 (2012).
[33] G. S. Redner, M. F. Hagan, and A. Baskaran, Structure and Dynamics of a Phase-Separating Active Colloidal Fluid, Phys. Rev. Lett. **110**, 055701 (2013).
[34] J. Palacci, S. Sacanna, A. P. Steinberg, D. J. Pine, and P. M. Chaikin, Living crystals of light-activated colloidal surfers, Science **339**, 936 (2013).
[35] I. Buttinoni, J. Bialké, F. Kümmel, H. Löwen, and C. Bechinger, Dynamical Clustering and Phase Separation in Suspensions of Self-Propelled Colloidal Particles, Phys. Rev. Lett. **110**, 238301 (2013).
[36] M. E. Cates and J. Tailleur, When are active Brownian particles and run-and-tumble particles equivalent? Consequences for motility-induced phase separation, Europhys. Lett. **101**, 20010 (2013).
[37] M. E. Cates and J. Tailleur, Motility-induced phase separation, Annu. Rev. Condens. Mat. Phys. **6**, 219 (2015).
[38] C. Reichhardt and C. J. O. Reichhardt, Active microrheology in active matter systems: Mobility, intermittency, and avalanches, Phys. Rev. E **91**, 032313 (2015).
[39] O. Chepizhko, E. G. Altmann, and F. Peruani, Optimal Noise Maximizes Collective Motion in Heterogeneous Media, Phys. Rev. Lett. **110**, 238101 (2013).
[40] O. Chepizhko and F. Peruani, Diffusion, Subdiffusion, and Trapping of Active Particles in Heterogeneous Media, Phys. Rev. Lett. **111**, 160604 (2013).
[41] C. Reichhardt and C. J. Olson Reichhardt, Absorbing phase transitions and dynamic freezing in running active matter systems, Soft Matter **10**, 7502 (2014).
[42] Cs. Sándor, A. Libál, C. Reichhardt, and C. J. Olson Reichhardt, Dynamic phases of active matter systems with quenched disorder, Phys. Rev. E **95**, 032606 (2017).
[43] T. Bertrand, Y. Zhao, O. Bénichou, J. Tailleur, and R. Voituriez, Optimized Diffusion of Run-and-Tumble Particles in Crowded Environments, Phys. Rev. Lett. **120**, 198103 (2018).
[44] C. Reichhardt and C. J. O. Reichhardt, Active matter transport and jamming on disordered landscapes, Phys. Rev. E **90**, 012701 (2014).
[45] C. J. Olson Reichhardt and C. Reichhardt, Avalanche dynamics for active matter in heterogeneous media, New J. Phys. **20**, 025002 (2018).
[46] N. Bain and D. Bartolo, Critical mingling and universal correlations in model binary active liquids, Nat. Commun. **8**, 15969 (2017).